Available online at www.sciencedirect.com
ScienceDirect
Ceramics International 33 (2007) 1299–1303
CERAMICS INTERNATIONAL
www.elsevier.com/locate/ceramint

Characteristics of $Ba_{0.8}Sr_{0.2}TiO_3$ ferroelectric thin films by RF magnetron sputtering

Wencheng Hu *, Chuanren Yang, Wanli Zhang, Guijun Liu

School of Micro-Electronics & Solid-State Electronics, University of Electronic Science and Technology of China, China

Received 10 October 2005; received in revised form 15 February 2006; accepted 27 April 2006
Available online 12 September 2006

Abstract

Ferroelectric $Ba_{0.8}Sr_{0.2}TiO_3$ (BST) thin films were deposited on $Pt/Ti/SiO_2/Si$ substrates via a modified RF magnetron sputtering by introducing the revolution of workholders. X-ray diffraction, Auger electron spectroscopy, atomic force microscope and electrical measurements were used to characterize BST thin films annealed at different temperatures. Smooth and dense surface with homogeneous grains (about 80 nm) was observed. The electrical measurement results showed BST films annealed at 650 °C have higher dielectric constant, lower loss tangent, lower leakage current and higher breakdown voltage. The curves of the temperature dependence of dielectric constant in different frequencies exhibit Curie transition at temperature around 19 °C. The remnant polarization and the coercive field are 4.1 $\mu C/cm^2$ and 60.9 kV/cm, respectively. This work clearly reveals the highly promising potential of BST thin films for application in uncooled infrared focal plane arrays.

Keywords: BST thin films; Ferroelectric; Dielectric constant; Dissipation factor

1. Introduction

Different functional thin films are attractive materials for applications in infrared uncooled focal plane arrays (UFPAs) [1–4]. UFPAs detectors can be divided into four types based on their operating principle [5]. These are resistive bolometer [6], pyroelectric sensor [7], dielectric bolometer [8] and thermoelectric detectors [9]. Perovskite thin films were promising dielectric and ferroelectric material with the properties of high dielectric constant, low leakage current density, and low dielectric loss [10]. Especially, ferroelectric BST thin films have large temperature coefficient of dielectric constants around their Curie temperatures (T_c) which is near room temperature and the T_c can be easily changed from 0 to 70 °C by adjusting the ratio of Ba/Sr [11]. Therefore, these films may be considered as the preferable candidates.

There were several previous works devoted to depositing methods of BST thin films, such as radio frequency sputtering [12,13], metal organic chemical vapor deposition [14,15], ion beam sputtering [16], and pulsed laser deposition (PLD) [17,18]. Of all the process, the most important is how to deposit a high quality BST ferroelectric thin film on substrate as the sensitivity of the sensor is directly originated from the property of the BST thin film. $Ba_{0.66}Sr_{0.34}TiO_3$ thin films by RF magnetron sputtering [19] and $Ba_{0.64}Sr_{0.36}TiO_3$ thin films by sol–gel process [20] had been investigated for UFPAs device applications. The aim of this work is to examine the microstructures and ferroelectric properties of $Ba_{0.8}Sr_{0.2}TiO_3$ on the substrate $Pt/Ti/SiO_2/Si$ by RF magnetron sputtering.

2. Experiment

2.1. Preparation of BST thin films

In our experiments, a modified RF magnetron sputtering device was used to ensure thickness uniformity of BST thin films. Schematic diagram of the RF magnetron sputtering system was shown in Fig. 1. The revolution of workholders was applied in our system. The velocities of the revolution and rotation of substrate were 2 and 4 rpm, respectively.

Prior to film deposition, 100 mm diameter ceramic target with composition of $Ba_{0.8}Sr_{0.2}TiO_3$ was fabricated using conventional ceramic processing. BST films were sputtered

* Corresponding author. Tel.: +86 28 83201171; fax: +86 28 83201632.
E-mail address: huwc@uestc.edu.cn (W. Hu).

0272-8842/$32.00
doi:10.1016/j.ceramint.2006.04.012

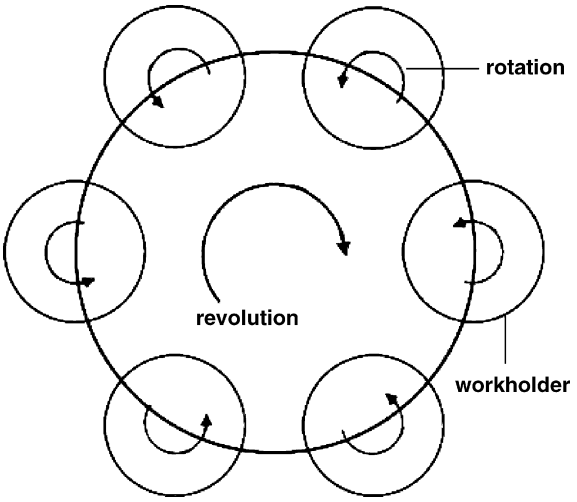

Fig. 1. Schematic diagram of the RF magnetron sputtering system.

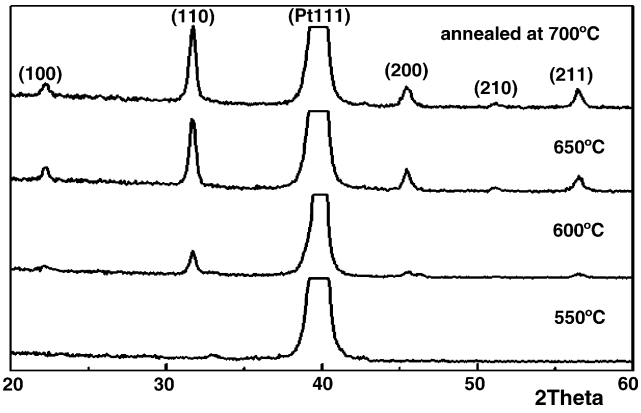

Fig. 2. XRD pattern of BST film grown on $Pt/Ti/SiO_2/Si$ substrates annealed at: (A) 550 °C for 5 min; (B) 650 °C for 5 min; (C) 650 °C for 15 min.

from the ceramic target onto $Pt/Ti/SiO_2/Si$ substrates in a mixture of Ar and O_2 gases. The substrate temperature was 300 °C, RF power was 120 W and the distance of source to substrate was 200 mm, gas flow ratio of Ar to O_2 was 2:1, and gas pressure was 0.5 Pa.

2.2. Characterization of BST thin films

The film thickness was measured by an ellipsometer. Ni-filtered Cu Kα radiation was used to determine the texture of the BST thin films by X-ray diffraction (Philips Xpert X-ray diffractometer). The surface morphologies of the BST films were analyzed by atomic force microscopy. In order to

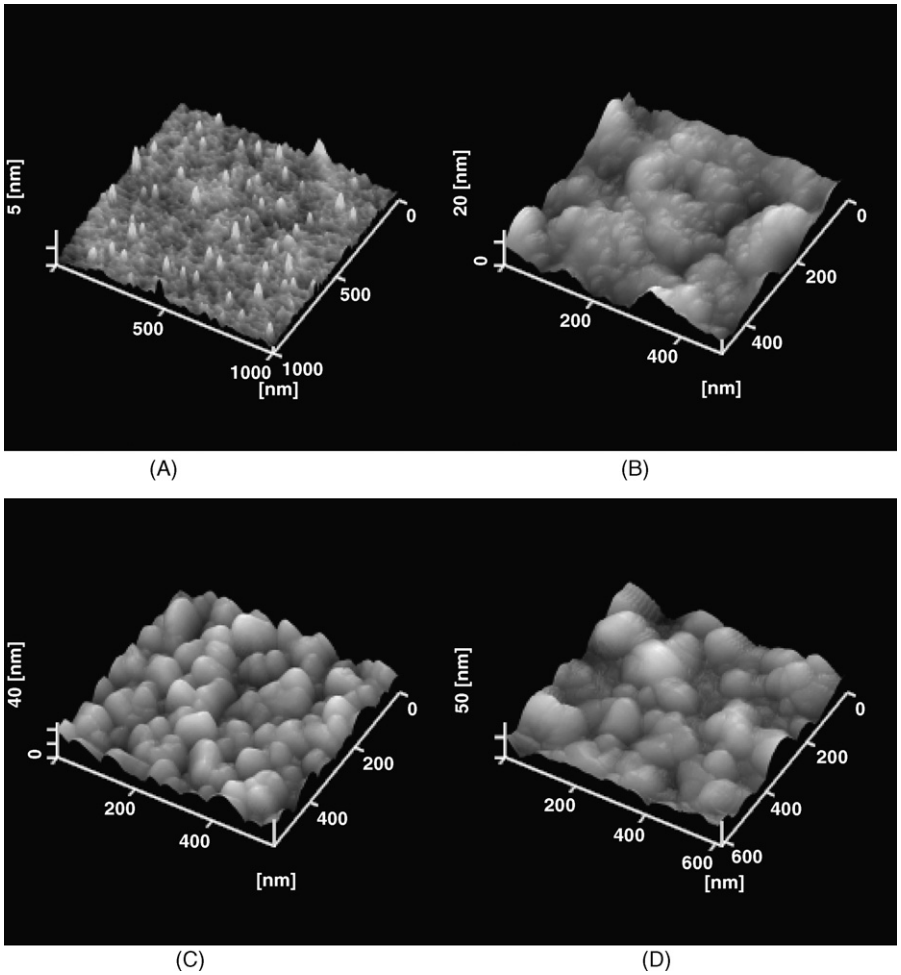

Fig. 3. Atomic force microscopy images of BST thin films grown on $Pt/Ti/SiO_2/Si$ substrates annealed at: (A) 550 °C for 15 min; (B) 600 °C for 15 min; (C) 650 °C for 15 min; (D) 700 °C for 15 min.

investigate chemical component, the BST/Pt/Ti/SiO_2/Si multilayer was analyzed by Auger electron spectroscopy (AES). Capacitance–temperature measurements were done at 100 Hz to 1 MHz using a HP4284A LCR meter. Ferroelectric properties of the BST thin films were evaluated with a RT66A ferroelectric test system.

3. Results and discussion

3.1. X-ray diffraction (XRD) analysis

The XRD patterns of the BST thin films annealed at 550, 600, 650 and 700 °C for 15 min are given in Fig. 2. The spectrum of the sample annealed at 550 °C shows no clear peaks belonging to BST crystalline and indicates the amorphous nature of the films. At 600 °C, the spectrum possessed the low (1 1 0) peak of perovskite BST and suggested an incomplete perovskite phase formed and the main of BST films was still amorphous state. As the annealing temperature increased, the peaks in the X-ray diffraction pattern became sharper, indicating that the formation of BST was better at high annealing temperature. Obviously, the XRD patterns of the BST thin films annealed at 650 and 700 °C are similar in sharp, and their FWHMs have a little difference which indicates the difference of grain size of BST thin films according to the Scherrer formula.

3.2. Atomic force microscopy (AFM) analysis

The surface morphologies of BST films observed with an atomic force microscopy are shown in Fig. 3. The surface roughnesses of these four samples are 0.832, 1.145, 2.847 and 3.513 nm, respectively. Fig. 3 (A) and (B) shows the BST thin film grown as the nanocrystals, and the main part can be seen in the image corresponding to amorphous state. The surface morphology is very homogeneous and a nearly flat surface. In the case of the images corresponding to the samples (B) and (C) annealed at 650 and 700 °C, the topography of the samples has changed in a drastic way. The surface is filled with quasi-spherical entities. The entities of sample (C) are uniform but sample (D) not, and the surface roughness of sample (B) is lower than sample (B), which can be interpreted as the higher annealing temperature of sample (D). On the other hand, it is also showed that the uniformity of grain size became worse at 700 °C. The surface morphologies of BST film estimated from AFM images are compared with the corresponding one obtained by X-ray diffraction patterns, achieving a good agreement that the BST thin films are annealed at 650 °C for 15 min. However, the mean grain size of the sample (C) is about 80 nm, which is typical of polycrystalline film.

3.3. AES analysis

AES Analysis is one of most methods to discuss the distributions of elements and stoichiometric of thin films. AES elemental depth profiles of BST thin films are shown in Fig. 4. In the AES concentration depth profiles, it was clear that the composition of the deposited structure was in good agreement with the planned one. Actually, the composition of the BST was different from the stoichiometric one due to heavy cation (Sr^{2+} and Ba^{2+}) generally displaying different sputtering rate than lighten cation (Ti^{4+}). The nearly stoichiometric near the interface of BST/Pt can be distinguished from the upper BST layer. The deviation from the stoichiometric composition in the interface layer can be attributed to the diffusing effect of Pt, which we have discussed in our previous research in details [21].

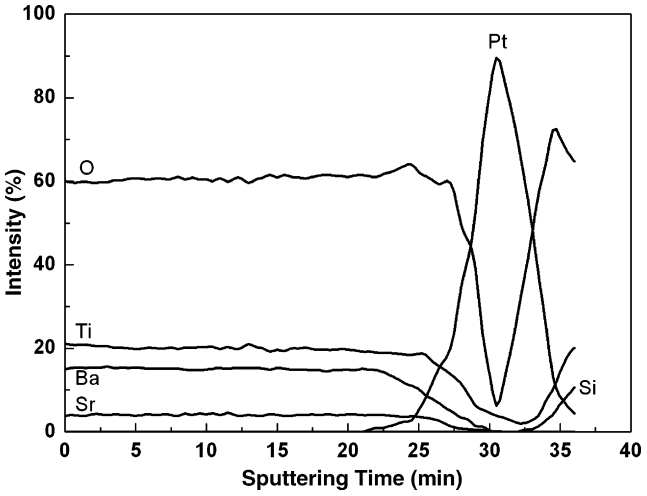

Fig. 4. AES elemental depth profiles of BST thin films annealed at 650 °C for 15 min.

3.4. Dielectric properties

The dielectric behavior of BST thin films (the thickness is about 300 nm) annealed at 650 °C for 15 min was measured in metal–BST–metal configuration with films sandwiched between the bottom platinum and top gold electrodes (the dot diameter is 0.5 mm). Figs. 5 and 6 showed the temperature dependence of dielectric constant and dissipation factor of BST thin films with different frequencies and zero bias, respectively.

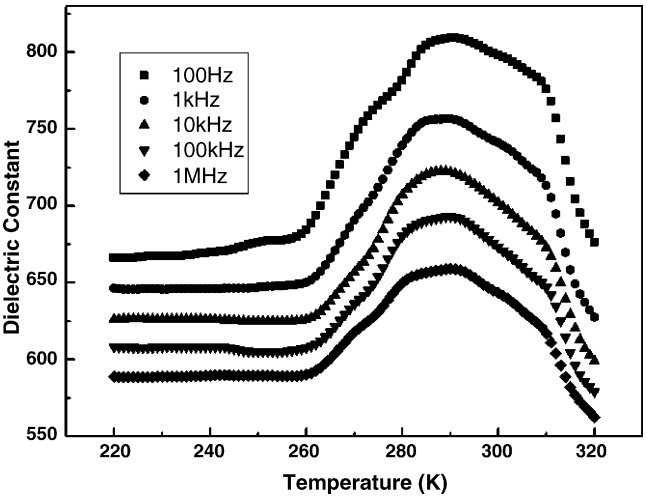

Fig. 5. The temperature dependence of the dielectric constant for the $Ba_{0.8}Sr_{0.2}TiO_3$ films annealed at 650 °C for 15 min.

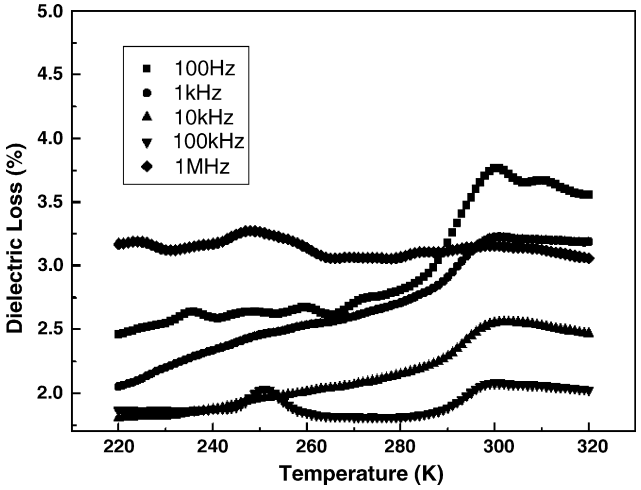

Fig. 6. The temperature dependence of the dielectric loss for the $Ba_{0.8}Sr_{0.2}TiO_3$ films at 650 °C for 15 min.

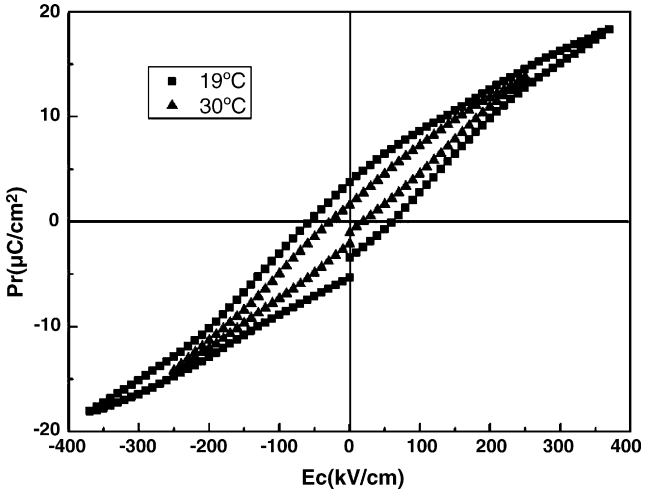

Fig. 7. Dielectric hysteresis loop of $Ba_{0.8}Sr_{0.2}TiO_3$ thin film.

The value of dielectric constant and the curves sharpness of the dielectric constant as a function of temperature were obviously higher those of previous references reported [11,12,22], which indicated that the pyroelectric coefficient is propitious to be enhanced according to its definition formula. When the electric field is a constant, the pyroelectric coefficient can be calculated by the equation as follows:

$$p = \varepsilon_0 E \frac{\mathrm{d}\varepsilon}{\mathrm{d}T}$$

where p is the pyroelectric coefficient, E, ε and ε_0 are electric field, dielectric constant and vacuum permittivity (=8.854 $\times 10^{-12}$ F/m). For the BST thin films, the contribution of first term is primary. Obviously, the sharper curve is advantageous to improve the pyroelectric performance of BST films.

As the frequency increased, the dielectric constant decreased homologically. The dielectric constant peak was about 292 K in the ε_r–T curve, which corresponded to a tetragonal to cubic phase transition. The dissipation factor was less than 4% the in temperature range from 200 to 320 K with different frequencies in the tg δ–T curve and showed a peak around 290 K. As the frequency increased, tg δ increased in the mass except 1 MHz. The least value of dissipation factors appears at 100 kHz.

3.5. Ferroelectric properties

The BST films annealed at 650 °C were used to evaluate the ferroelectric properties. Fig. 7 showed the P–E hysteresis loops of the samples measured at 292 and 320 K, and their shapes displayed incomplete saturation. It was also found that the P–E plot showed a hysteresis loop with counter clockwise trace indicating the ferroelectric behavior of the BST films. Obviously, BST thin films measured at 292 K possessed the more advanced ferroelectricity. Once the measurement temperature was raised to 320 K, the loop became narrow. It was considered that the measurement temperature was above Curie point, and the tetragonal phase had translated to cubic phase and the ferroelectric properties became worse. The remnant polarization and a coercive field of the $Ba_{0.8}Sr_{0.2}TiO_3$ thin films measured at 292 K are 4.1 μC/cm^2 and 60.9 kV/cm, respectively.

3.6. Leakage current characteristics

The J–E characteristics of BST thin films as a function of the square root of applied electric field were shown in Fig. 8. The leakage current measured at 320 K was higher and breakdown field was lower compared with it measured at 292 K. The lower temperature leaded to improve the leakage current characteristics of BST thin films. The decrease in leakage current density can be attributed to thermal electric activity. The linear relationship of the log J versus $E^{1/2}$ curves showed in a good agreement with the Schottky thermionic emission mode at the higher electric field [23]:

$$I_{SK} = AT^2 \exp\left[\frac{-q(\phi_b - \sqrt{qE/4\pi\varepsilon_i})}{kT}\right]$$

where A, q, ϕ_b, E and ε_i are the effective Richardson constant, the charge, the Schottky barrier height, the electric field and the

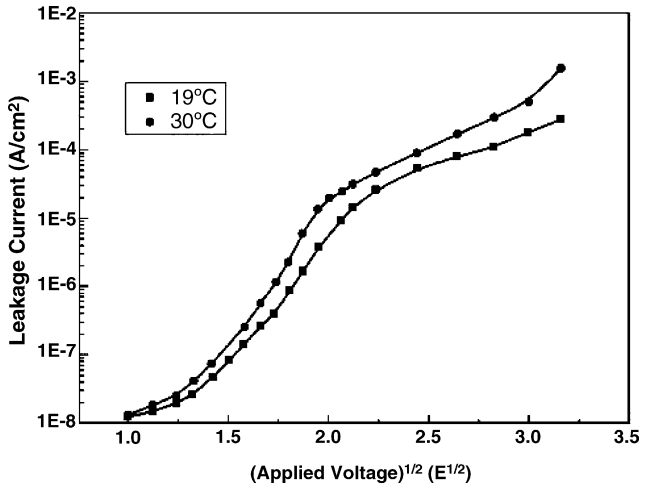

Fig. 8. Leakage current density as a function of square root of applied field for thin films.

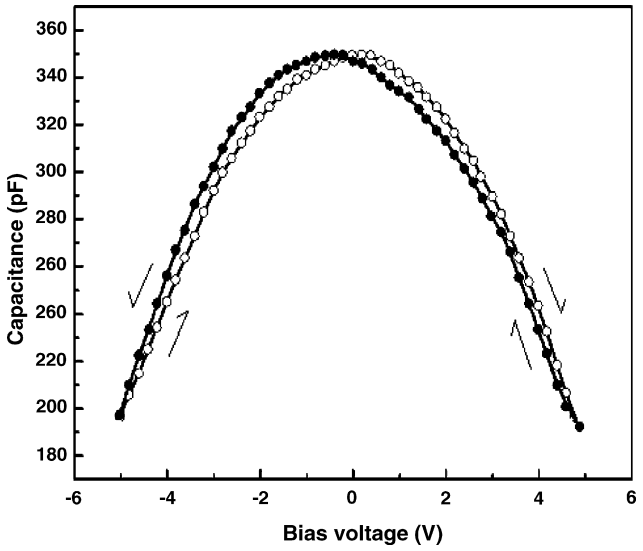

Fig. 9. *C–V* curve of $Ba_{0.8}Sr_{0.2}TiO_3$ thin film at the frequency of 100 kHz.

insulator dynamic permittivity. This result indicated that the conduction mechanism in these BST films at the higher electric field followed the Schottky thermionic emission process.

3.7. Dielectric constant–voltage characteristic

In Fig. 9, the dependence of the capacitance as a function of the voltage showed a strongly non-linear character, and two peaks characterizing spontaneous polarization switching can be seen in the figure. Therefore, the films' butterfly-shaped *C–V* curves indicated that the films have a ferroelectric nature. The capacitance changed from 193 to 349 pF with the applied voltage in the −5–5 V range at a frequency of 100 kHz, which was considerable large and will make it easier to readout the capacitance change in application of dielectric type IR sensors.

4. Summary

The high dielectric constant $Ba_{0.8}Sr_{0.2}TiO_3$ (BST) ferroelectric thin films on the substrate $Pt/Ti/SiO_2/Si$ used for uncooled infrared focal plane arrays with a remnant polarization of 4.1 $\mu C/cm^2$ and a coercive field of 60.9 kV/cm had been successfully prepared by a modified RF magnetron sputtering system. X-ray diffraction and atomic force microscopy investigations showed that the BST films exhibit a tetragonal structure and consist dominantly of large column or grains of about 80 nm in diameter. AES elemental depth profiles of BST thin films showed the uniformity of composition. The curves of the temperature dependence of dielectric constant in different frequencies exhibited Curie transition at temperature around 19 °C. The dissipation factors of BST thin films at 100 kHz were less than 0.02.

References

[1] V.R. Mehta, S. Shet, N.M. Ravindra, et al. J. Electron. Mater. 34 (2005) 484.
[2] L. Dong, R. Yue, L. Liu, Int. J. Infrared Millimeter Waves 24 (2003) 1351.
[3] Y.-K. Park, B.-K. Ju, H.-w. Park, et al. Proc. SPIE—Int. Soc. Opt. Eng. 3892 (1999) 356.
[4] S. Chen, H. Ma, S. Wang, et al. Thin Solid Films 497 (2006) 267.
[5] M. Nada, Sensor Lett. 3 (2005) 194.
[6] K. Hayashi, E. Ohta, H. Wada, J. Vac. Sci. Technol. A 19 (2001) 2905.
[7] R.W. Whatmore, R. Watton, Ferroelectrics 236 (2000) 259.
[8] S.-J. Liu, J.-H. Chu, Proc. SPIE—Int Soc. Opt. Eng. 5640 (2005) 49.
[9] M.T. Rodrigo, J. Diezhandino, G. Vergare, et al. Proc. SPIE—Int. Soc. Opt. Eng. 5251 (2004) 97.
[10] L. Goux, M. Gervais, A. Catherinot, et al. J. Non-Cryst. Solids 303 (2002) 194.
[11] H. Xu, H. Zhu, K. Hashimoto, et al. Vacuum 59 (2000) 628.
[12] V. Reymond, D. Michau, S. Rayan, et al. Ceram. Int. 30 (2004) 1085.
[13] Y.-F. Kuo, T.-Y. Tseng, Mater. Chem. Phys. 61 (1999) 244.
[14] S. Regnery, P. Ehrhart, F. Fitsilis, et al. J. Eur. Ceram. Soc. 24 (2004) 271.
[15] Y.-S. Min, Y.J. Cho, D. Kim, et al. Adv. Mater. 13 (2001) 146.
[16] Y.R. Liu, P.T. Lai, B. Li, et al. Mater. Chem. Phys. 94 (2005) 114.
[17] L. Rahbapiyari, A.R. Janes, O.P. Thakur, et al. Mater. Sci. Eng. B 117 (2005) 5.
[18] S.-J. Lee, K.-Y. Kang, S.-K. Han, et al. Integr. Ferroelectrics 24 (1999) 33.
[19] J.S. Lee, J.-S. Park, J.-S. Kim, et al. Jpn. J. Appl. Phys. 38 (1999) 574.
[20] L. Dong, R. Yue, L. Liu, et al. Int. J. Infrared Millimeter Waves 24 (2003) 1341.
[21] W. Hu, C. Yang, W. Zhang, et al. J. Sol–Gel Sci. Technol. 39 (2006) 293.
[22] B. Su, J.E. Holmes, C. Meggs, et al. J. Eur. Ceram. Soc. 23 (2003) 2699–2703.
[23] X.F. Chen, W.G. Zhu, O.K. Tan, Mater. Sci. Eng. B 77 (2000) 177.